Original Article

Predicting the Response of Patients Treated with ^{177}Lu-DOTATATE Using Single-photon Emission Computed Tomography–Computed Tomography Image-based Radiomics and Clinical Features

Abstract

Background: In this study, we want to evaluate the response to Lutetium-177 (^{177}Lu)-DOTATATE treatment in patients with neuroendocrine tumors (NETs) using single-photon emission computed tomography (SPECT) and computed tomography (CT), based on image-based radiomics and clinical features. **Methods:** The total volume of tumor areas was segmented into 61 SPECT and 41 SPECT-CT images from 22 patients with NETs. A total of 871 radiomics and clinical features were extracted from the SPECT and SPECT-CT images. Subsequently, a feature reduction method called maximum relevance minimum redundancy (mRMR) was used to select the best combination of features. These selected features were modeled using a decision tree (DT), random forest (RF), K-nearest neighbor (KNN), and support vector machine (SVM) classifiers to predict the treatment response in patients. For the SPECT and SPECT-CT images, ten and eight features, respectively, were selected using the mRMR algorithm. **Results:** The results revealed that the RF classifier with feature selection algorithms through mRMR had the highest classification accuracies of 64% and 83% for the SPECT and SPECT-CT images, respectively. The accuracy of the classifications of DT, KNN, and SVM for SPECT-CT images is 79%, 74%, and 67%, respectively. The poor accuracy obtained from different classifications in SPECT images (≈64%) showed that these images are not suitable for predicting treatment response. **Conclusions:** Modeling the selected features of SPECT-CT images based on their anatomy and the presence of extensive gray levels makes it possible to predict responses to the treatment of ^{177}Lu-DOTATATE for patients with NETs.

Keywords: *Lutetium-177-DOTATATE, neuroendocrine tumors, radiomics, single-photon emission computed tomography, single-photon emission computed tomography–computed tomography*

Submitted: 05-Nov-2023 **Revised:** 01-May-2024 **Accepted:** 27-May-2024 **Published:** 16-Oct-2024

Baharak Behmanesh[1], Akbar Abdi-Saray[1], Mohammad Reza Deevband[2], Mahasti Amoui[3], Hamid R. Haghighatkhah[4], Ahmad Shalbaf[2]

[1]Department of Nuclear Physics, Urmia University, Oroumieh, [2]Department of Biomedical Engineering and Medical Physics, School of Medicine, Shahid Beheshti University of Medical Sciences, [3]Department of Nuclear Medicine, School of Medicine, Shohada-e Tajrish Hospital, Shahid Beheshti University of Medical Sciences, [4]Department of Radiology and Medical Imaging Center, School of Medicine, Shohada-e Tajrish Hospital, Shahid Beheshti University of Medical Sciences, Tehran, Iran

Address for correspondence:
Dr. Mohammad Reza Deevband, Department of Biomedical Engineering and Medical Physics, School of Medicine, Shahid Beheshti University of Medical Sciences, Tehran, Iran.
E-mail: mdeevband@sbmu.ac.ir
Dr. Ahmad Shalbaf, Department of Biomedical Engineering and Medical Physics, School of Medicine, Shahid Beheshti University of Medical Sciences, Tehran, Iran.
E-mail: shalbaf@sbmu.ac.ir
Dr. Akbar Abdi-Saray, Department of Nuclear Physics, Urmia University, Oroumieh, Iran.
E-mail: ak.abdi@urmia.ac.ir

Access this article online

Website: www.jmssjournal.net

DOI: 10.4103/jmss.jmss_54_23

Quick Response Code:

Introduction

Neuroendocrine tumors (NETs) are rare malignancies[1,2] that are divided into three groups according to the World Health Organization (WHO) classification based on the mitotic rate and Ki-67 index. The first group had a Ki-67 index of <3% (Group 1), the second group had a Ki-67 index between 3% and 20% (Group 2), and the third group had a Ki-67 index >20% (Group 3).[3] Peptide receptor radionuclide therapy (PRRT) is a novel approach for the treatment of this type of cancer, in which radionuclide-labeled peptides bind to somatostatin receptors. Neuroendocrine cells with somatostatin receptors are targeted by lutetium-177 (^{177}Lu)-labeled somatostatin analog octreotate, and the DNA of these cells is destroyed through radioactive decay.[4-6] ^{177}Lu has a half-life of 6.73 days, emits gamma rays (113 keV [6.4%] and 208 keV [11%]), and is used for imaging purposes. It is used to treat patients with NET as it also emits beta particles (497 keV) with a penetration range of about 2 mm in the human body, which decomposes into (^{177}Hf) through the emission of these particles.[7] With the injection of ^{177}Lu-DOTATATE, the absorption of radionuclides into the tumor is increased compared to that in healthy tissues.

The use of response evaluation criteria in solid tumors, biochemical evaluation of tumors, and other approaches are considered expensive and time-consuming.[8] Radiomics

How to cite this article: Behmanesh B, Abdi-Saray A, Deevband MR, Amoui M, Haghighatkhah HR, Shalbaf A. Predicting the response of patients treated with ^{177}Lu-DOTATATE using single-photon emission computed tomography–computed tomography image-based radiomics and clinical features. J Med Sign Sens 2024;14:28.

is a novel and low-cost method for studying medical images, in which various image features that are not visible to the human eye are extracted.[9] In this approach, each pixel of the image contains features of the tumor that are related to the treatment response.[10] Radiomics involves several steps, including image acquisition, image segmentation of the region of interest, feature extraction, feature selection, modeling, and evaluation.[11,12] Radiomics features are based on the intensity, morphology, and texture of the tumor phenotype. In recent years, many researchers have used a combination of radiomic features and artificial intelligence (AI) for various purposes, such as predicting the histology of cancer types, grading neuroendocrine cancers, and predicting survival.[8,9,13,14] Ma *et al*. studied 41 patients with pancreatic NET (PNET) with disease Grades 1, 2, and 3. They extracted 107 features from ^{68}Ga-DOTATATEPET/computed tomography (CT) images and screened 12 radiomic features according to Pearson's correlation coefficient. Using logistic regression modeling, they were able to predict the grade of tumors with an area under the curve (AUC) of 0.97%.[15] In 2023, Alibabaei *et al*. extracted features based on radiomics (GLCM) of magnetic resonance images (MRI) of glioblastoma patients with MATLAB. They were able to obtain the important distinctive characteristics of the response to the treatment and the progression of the disease by statistical analysis by the collected data from all groups were imported to Statistical Package for Social Sciences (SPSS) for Windows software (SPSS Inc., Chicago, IL, USA).[16] Dehghani *et al*. segmented brain tumors using fluid-attenuated inversion recovery (FLAIR), T1-weighted (T1W), T2-weighted, and T1W (T1ce) magnetic resonance. Their method was automated and based on deep learning. Their dataset included 370 samples with specific tumor masks. They concluded that the quantitative evaluation of single-channel models with FLAIR sequence has a higher segmentation accuracy compared to its counterparts with a Dice index of 0.10 ± 0.77.[17]

In 2022, Xu *et al*. conducted a study using logistic regression model features of MRI to differentiate nonhypervascular PNETs from pancreatic ductal adenocarcinomas (PDACs). The results with high model accuracy showed that these features could distinguish hypervascular PNETs from PDACs before surgery.[13] In the same year, Zhang *et al*. also used an random forest (RF) algorithm on the radiomic features of CT images to differentiate PDAC from PNET. They achieved this goal with an accuracy, sensitivity, and specificity of 0.742, 0.934, and 0.930, respectively.[14] In 2022, we used machine learning to investigate CT images of NET patients who underwent PRRT. We found that the features extracted using the extreme gradient boosting pattern in combination with the RF classifier can predict the response to treatment with an accuracy of 89%.[18]

In recent years, much research has been done in the field of grading different tumors, evaluating the behavior of tumors, and predicting the response to treatment using different medical images with AI. In this research, we used different machine-learning algorithms to predict the response to treatment with ^{177}Lu-DOTATATE in patients with NETs. What distinguishes our research from the work of others is the use of features extracted from single-photon emission CT (SPECT) and SPECT-CT images for this purpose.

Materials and Methods

Patient characteristics

This study included patients with NETs whose disease was confirmed by pathological tests. The "Ki-67" index was measured using immunohistochemistry and was determined based on the WHO classification. Ki-67, or the mitotic index, is a way of describing how many cells are dividing and is considered a clinical feature.[19] A total of 22 patients (12 female and 12 male) were selected for SPECT-CT imaging. The average ages of the male and female patients were 56.54 and 57.18 years, respectively. The disease of the selected patients was proven by pathological tests. None of them had received any other treatment such as radiotherapy or chemotherapy before PRRT treatment with ^{177}Lu-DOTATATE. Three patients died during treatment. A summary of the initial patient information is shown in Table 1.

Lutetium-177-DOTATATE therapy

Each patient received 6.7–7.4 GBq of ^{177}Lu-DOTATATE four to six times with an interval of 2 to 3 months. However, depending on the patient's physical condition and the specialist's diagnosis, the activity could be lower.

After each treatment period, the patients were asked several questions about "fatigue," "drowsiness," "nausea," and other symptoms. The Edmonton Symptom Assessment System-Revised (ESAS-R) scale was used to answer the questions. In other words, these evaluations were performed to determine the effect of treatment on the patient's quality of life. The patients were instructed to rate their condition on a scale of 0 to 10. Zero denotes the best state; the farther away from 0, the worse the physical condition of the patient. The scores for each course were compared with those for the first course of treatment. If the patient's condition changes by 25%, it implies no response to treatment. A score between 25% and 75% indicated a relative response to treatment, whereas a score above 75% indicated a complete response to treatment.

Single-photon emission computed tomography imaging and follow-up

SPECT images were taken 24 h after radiopharmaceutical injection to determine the extent of radiopharmaceutical uptake into the lesion and the location of the lesion. All SPECT images of the patients were obtained using a SIEMENS gamma camera model 2016. They all had similar image dimensions (128×128) and 4.8 mm^3 voxel

sizes. Uptake was not observed in areas with healthy tissue. During the treatment, four SPECT images were obtained for each patient. Only the first image of the patient was used to compare the condition of the patient in the next imaging session. Therefore, the initial images were discarded, and the radiomic features of the next three images were used to predict the response to treatment. Basically, there should be 66 SPECT images obtained from 22 patients. However, because three patients died during treatment, their images remained incomplete. Thus, the total number of SPECT images was reduced to 61.

Single-photon emission computed tomography–computed tomography acquisition

A baseline CT image was obtained from each patient before starting treatment. Two CT images were also taken 6 and 12 months after treatment. CT images of patients were taken in different clinics with different protocols. All images were resampled with dimensions of 512 × 512 and 1 mm^3 voxel sizes by three-dimension (3D) Slicer software. CT images of some patients were used in our previous research. In this study, patients' CT images were used for fusion with their SPECT images to obtain SPECT-CT images.[18] Furthermore, the 3D Slicer software was used to fuse the images. First, all images were converted from DICOM to NRRD format. "Landmark Registration" part of the "Registration" module was selected for fusing images. The CT image was defined as a fixed image and the SPECT image as a moving image. For the two images to overlap completely, it was necessary that the dimensions of the two images were adjusted manually and identically using the "Volume" module. This module has "Image Dimensions," "Image Spacing," and "Image Origin" tools that can be accessed for this purpose. After this step, the "Translation" and "Rotation" sections of the "Transform" module were used to make the tumoral region of the SPECT image fall exactly on the same region in the CT image.

The first CT image of each patient was fused with the SPECT image of the first cycle, the second with the SPECT image of the third cycle, and the last with the SPECT image of the fourth cycle. The initial SPECT-CT image was only used for comparison with subsequent periodic images. Therefore, the initial SPECT-CT images of the patients were discarded to determine radiomic features, and the next two images were used for this purpose. In total, 44 SPECT-CT images from 22 patients were used to determine the radiomics features. As three patients died during the treatment, their images remained incomplete. In total, 41 SPECT-CT images were obtained for the radiomics analysis of patients with NETs.

Table 1: Characteristics of the patients included and the single-photon emission computed tomography and single-photon emission computed tomography–computed tomography images

Characteristic	Patients number
Patients under study for SPECT images	
Male (age average)	11 (57.18)
Female (age average)	11 (56.54)
The range of patient's age	38–81
Dead patients	3
IHC result	
Ki-67<3%	8
3% < Ki-67<20%	9
Ki-67≥20%	2
Unknown Ki-67	3
The primary site of the tumor	
Pancreas	6
Stomach	2
Small intestine	4
Pelvis	1
Lungs	5
Liver	1
Metastatic NETs of unknown origin	5
Site of metastasis	
Pelvis	3
Liver	16
Lungs	4
Lymph nodes	6
Bone	5
Breast	1
Thyroid	1

IHC – Immunohistochemistry; Ki-67 – The Ki-67 index, or mitotic index, describes the number of dividing cells; SPECT – Single-photon emission computed tomography; NETs – Neuroendocrine tumors

Tumor segmentation

On the SPECT and SPECT-CT images, areas showing radiopharmaceutical uptake into the lesion were segmented under the supervision of a nuclear physician. Segmentation was performed using the 3D Slicer software version 4.11 (https://www.slicer.org). Figure 1a and c

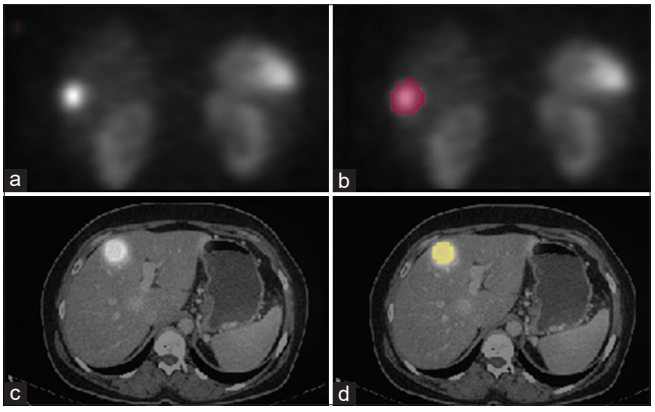

Figure 1: (a) Single-photon emission computed tomography (SPECT) image of a patient with neuroendocrine tumors (NETs). (b) Segmentation of the region of interest in the SPECT image. (c) Single-photon emission computed tomography–computed tomography (SPECT-CT) image of a patient with NETs. (d) Segmentation of the region of interest in the SPECT-CT image

show examples of the SPECT and SPECT-CT images, respectively. Figure 1b and d show the segmentation of the desired areas.

Radiomic and clinical features extraction

After specifying the region of interest in the medical images using 3D Slicer software, radiomics features were extracted. Radiomic features can reveal differences in tumor phenotypes.[20] Intensity (n = 18), texture (n = 75), shape (n = 14), and transform-based (wavelet) features (n = 744)[17,18] were extracted. In wavelet transforms, despite preserving spatial information, the image is converted into the frequency domain.[21] Age, sex, number of lesions, and the largest and smallest lesions were qualitatively evaluated in both SPECT-CT and SPECT images, and their values were placed separately in the SPECT-CT and SPECT datasets as other features (n = 5). In both images, the absorption intensity was another factor that was considered. Mild, moderate, and high uptake levels were separated, and their percentages were calculated. These features were added to the SPECT and SPECT-CT datasets as additional features (n = 3).

We also extracted clinical features. In each treatment period, patients were tested before receiving radiopharmaceuticals. The tests include "white blood cell count," "red blood cell count," "hemoglobin (Hb) test," "creatinine blood test (Cr)," "platelet count," "blood urea nitrogen," "bilirubin test," "alkaline phosphatase level test," "(alanine aminotransferase or serum glutamic-pyruvic transaminase)," and "aspartate aminotransferase (AST or serum glutamic oxaloacetic transaminase [SGOT])." These tests and "Ki-67" were considered clinical features. The values of the clinical features (n = 11) and injection activity injected activity (n = 1) in patients during each period were added to the quantitative features. The activity injected into the patients after some time showed its effect on the rate of lesion healing (shrinkage or disappearance of the lesion) on CT images. Therefore, "activity" was also considered a feature in the CT dataset.

Feature normalization

After extracting the features, we found that the ranges of their values differed significantly. This difference reduces the prediction and performance of the model. Therefore, before selecting the features and classification, the minimum–maximum normalization (feature scaling) method was used. This method is a simple way to normalize the data. The minimum-maximum normalization formula is as follows:

$$x' = \frac{x - x_{min}}{x_{max} - x_{min}} \quad (1)$$

Where x is an original value and x' is the normalized value. Using this method, the values of the features were scaled in the range of 0 to 1.[22]

Feature selection

After data normalization, the next step in the radiomics method is feature selection. The number of extracted features (871 features) was much greater than the number of samples (61 samples in SPECT and 41 samples in SPECT-CT), which increased the machine learning time and the overfitting of the model. To overcome this problem, feature reduction techniques were used. In this study, the minimum redundancy - maximum relevance (mRMR)[23,24] was used to select important features. The mRMR method measures the relationship between each attribute and target variable based on mutual information. Mutual information is defined as follows:

$$I(X, Y) = \iint P(x, y) \log \frac{P(x, y)}{P(x)P(y)} dx\, dy \quad (2)$$

where x and y represent random variables. $P(x, y)$, $P(x)$, and $P(y)$ are probabilistic density functions. The algorithm holds the most relevant features and removes the remaining features (maximum relevance).

$$\text{Rel(s)} = \frac{1}{S} \sum_{t \in s} I(X_t, Y) \quad (3)$$

"S" is a feature set. In the next step, the relationship between each feature is evaluated, the variables that are strongly related to each other are removed, and only one of them is retained (minimum-redundancy).

$$\text{Red}(s) = \frac{1}{S^2} \sum_{t \in s} I(X_t, X_s) \quad (4)$$

After feature selection, a t-test was performed to measure the relationship between each feature and the target (response to treatment), and a $P < 0.05$ was considered to be statistically significant.

Classification and modeling

One of the types of machine learning methods is supervised learning. Supervised learning is divided into classification and regression.[25] In this research, the machine learning method of classification and labeling was used. In the study of SPECT-CT and SPECT images, the labels obtained from the "ESAS-R" scale were used to predict the response to treatment using the clinical and radiomic process in the classification problem. "Nonresponse to treatment," "partial response to treatment" and "complete response to treatment" were marked with "1", "2" and "3" labels, respectively. For the patients who died in the middle of the treatment, label 1 was assigned, meaning no treatment.

To categorize the data into different classes, a support vector machine (SVM), decision tree (DT) with Gini coefficient, RF, and k-nearest neighbors (KNN) were used.

SVM searches for the hyperplane that has the most margins with the classes and minimizes errors. The data cannot always be separated linearly. Therefore, in this category, different kernel tricks are used, and the data are projected onto a higher dimensional space using a function.[26] DT is one of the most

powerful supervised machine learning methods. Finding the root is the first step in forming a tree, which is obtained with two different "Gini" and "Entropy" coefficients. A tree is a set of nodes and branches, each representing a feature. One of the advantages of a DT is that it can be interpreted and is suitable for analyzing large amounts of data in a short time.[27] The RF algorithm stands out among machine learning algorithms because of its good performance with multiclass and unbalanced data. An RF is a set of trees, where each tree provides a label for a new sample. The final label was determined by the majority vote of the trees.[27] Finally, KNN is the simplest classifier used for both regression and classification. However, they are primarily used to classify issues. The KNN algorithm uses a KNN data label to identify new data classes.[28] All codes were written in Python version 3.8.4 (https://www.python.org).

Model performance evaluation

The receiver operating characteristic (ROC), and AUC are commonly used to evaluate the performance of binary classifiers. However, they are unsuitable for assessing multiclass classifiers, and evaluations based on confusion matrixes are preferred. In this study, confusion matrixes were used to obtain the sensitivity (SN), specificity (SP), and accuracy (ACC) criteria of the model.[29]

$$SN = \frac{TP}{TP + FN} \quad (5)$$

$$SP = \frac{TN}{TN + FP} \quad (6)$$

$$ACC = \frac{TP + TN}{TP + TN + FP + FN} \quad (7)$$

Sensitivity is the ability of a model to find "no response to treatment" cases. Specificity is the ability of a model to find "response to treatment" cases. The accuracy is the ability of a model to correctly differentiate between "no response to treatment" and "response to treatment" cases. To compensate for the small number of samples, we used the K-fold cross-validation strategy to study the machine learning algorithms. Based on the lowest number of labels in the classifications, the K-fold was considered to be nine for the SPECT and SPECT-CT attributes. Using this strategy made our results generalizable. The dataset was divided into (K = 9) folds. The models were trained and evaluated nine times. Each time, a different fold was used as a validation set. The performance measures from each class were averaged to estimate the generalization performance of the model.

Results

Of the total clinical and radiomic features (871 features) extracted from 41 SPECT-CT images (taken from 22 patients), eight features that were closely related to the prediction of response to treatment were selected using the mRMR method [Figure 2]. All four radiomic features

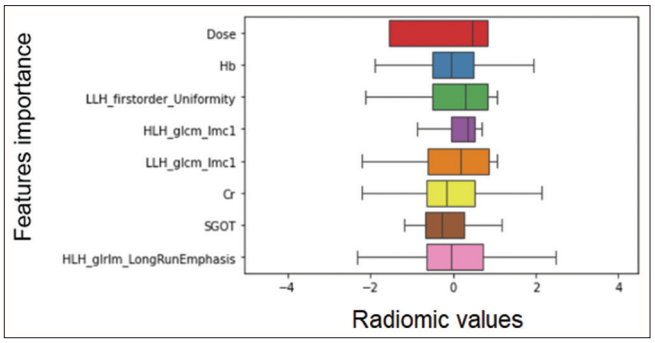

Figure 2: Obtained features by the mRMR algorithm in order of importance for single-photon emission computed tomography images. mRMR: Minimum redundancy - maximum relevance. SGOT: Serum glutamic oxaloacetic transaminase

were wavelet transformed. The other four clinical features are "activity injected into patients (dose)," "Hb," "Cr," and "AST (SGOT)." "Cr" is an indicator of kidney function. The "SGOT" test is used to diagnose liver failure. All features had a $P < 0.01$.

Among the 871 features extracted from 61 SPECT images, ten features that had the strongest relationship with the prediction of response to treatment were selected based on the mRMR pattern [Figure 3]. All features were transform-based wavelet features. Nine features had a $P < 0.01$. The "LLH_gldm_Large Dependence High Gray Level Emphasis" feature had a $P = 0.2$.

It should be noted that initially, 20 important features were selected from both SPECT and SPECT-CT images using the mRMR pattern. Only the most effective features were retained in the treatment using a trial-and-error method and feature modeling. In other words, only ten features were obtained for the SPECT images, and eight features were obtained for the SPECT-CT images.

The features selected from the SPECT-CT, and SPECT images were separately modeled using classifiers (DT, RF, KNN, and SVM). The results of the evaluation of the classifiers are shown in Figures 4 and 5 with a bar plot. In these diagrams, the horizontal and vertical axes represent the model and its performance in terms of percentages The red, green, and blue columns indicate the accuracy, specificity, and sensitivity of the models, respectively. The number of trees (n-estimator) in the RF algorithm was assumed to be 100. The best result for the KNN algorithm was obtained by setting the number of neighbors to (K = 3) for the SPECT and SPECT-CT data.

The combination of mRMR features obtained from both the SPECT and SPECT-CT images with the RF and DT classifiers was more accurate than the other predictive models. According to Figure 4, the accuracy, specificity, and sensitivity of the RF and DT models were 83%, 94%, and 77% and 79%, 93%, and 77% for the SPECT-CT features, respectively. In the SPECT images [Figure 5], evaluation of the features obtained from the mRMR pattern

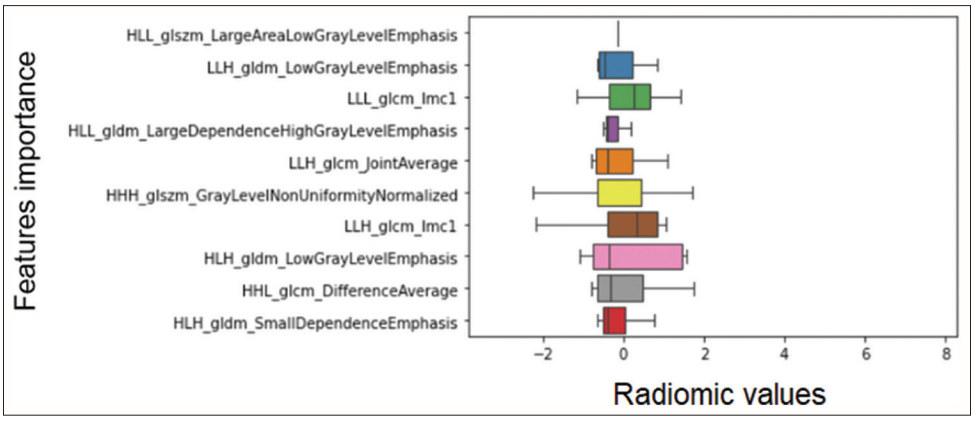

Figure 3: Obtained features by the mRMR algorithm in order of importance for single-photon emission computed tomography images. mRMR: Minimum redundancy - maximum relevance

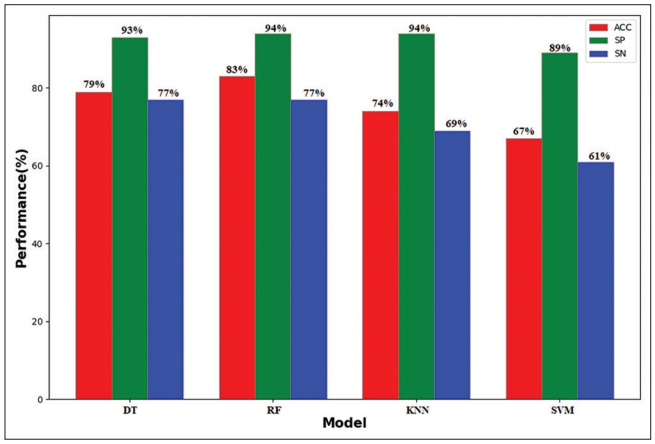

Figure 4: Barplot of the performance of the predictive models for single-photon emission computed tomography–computed tomography features in order of accuracy, specificity, and sensitivity. DT: Decision tree, RF: Random forest, KNN: K-nearest neighbor, SVM: Support vector machine

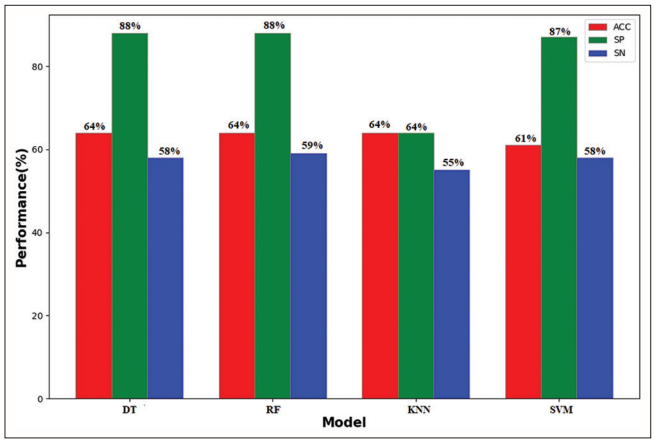

Figure 5: Barplot of the performance of the predictive models for single-photon emission computed tomography features in order of accuracy, specificity, and sensitivity. DT: Decision tree, RF: Random forest, KNN: K-nearest neighbor, SVM: Support vector machine

in combination with the machine learning algorithms showed that the performances of the RF and DT models were almost the same. The accuracy of both models in predicting response to treatment was 64%.

Discussion

After extracting and integrating the quantitative features of SPECT and SPECT-CT images with clinical factors, the mRMR algorithm was used to select features related to treatment response. The reason for its use is the popularity of the algorithm in medical studies,[30,31] its high computational accuracy, and its feature ranking. The SVM, DT, RF, and KNN were used to categorize the data into different classes.

According to Figure 2, the "dose" was the biggest factor influencing the response to the ^{177}Lu-DOTATATE treatment. Based on the *P* value (mentioned in the result section) for this feature in the SPECT-CT dataset, it can be said that it is 99.99% related to the response to treatment. In addition, the quantitative features extracted from the images are important factors.

Figure 3 shows that the quantitative features obtained from the SPECT images were all transform-based (wavelet) types, whereas in the SPECT-CT images [Figure 2], there were four features of this type. In the SPECT-CT features, "Hb," "SGOT," and "Cr" were also among the factors affecting treatment. The clinical features of patients in each course of treatment influence their response to treatment. Cr measures kidney function, and SGOT is used to diagnose the liver failure. "Hb" is also used to determine the amount of Hb in the blood. Radiomics can identify tumor phenotypes based on these features.[32] In the studies of Laudicella *et al*.,[10] which used the radiomics process to predict the response in GEP-NETs under ^{177}Lu (DOTATOC) PRRT, the features of "skewness," and "kurtosis" were considered effective features in response to treatment.

In our study, these features (kurtosis and skewness) were not selected using the mRMR pattern as important features in the SPECT and SPECT-CT images. In contrast to their results, in the SPECT-CT hybrid image, radiomic features (first order uniformity, glcm-informational measure of correlation [IMC1], and glrlm-Long Run Emphasis [LRE]) were selected as effective features

in response to treatment. "Uniformity" (corresponding to first-order uniformity) is used to measure the sum of the squares of any intensity value and is a measure of homogeneity. Higher uniformity indicates greater homogeneity. "IMC1" is a type of correlation that quantifies tissue complexity. "LRE" represents textures with a larger structure. An important common denominator between our study and that of Laudicella *et al*.[10] was that the Ki-67 index was not selected as an effective attribute. This finding is clinically significant. This means that the degree of the tumor cannot be determined based on the response to treatment.

Liberini *et al*.[33] used the radiomic features of ^{68}Ga/DOTATOC positron emission tomography (PET)/CT images for the PRRT outcomes of two patients. They found the "glrlm-LRE" feature to be effective, and they came to a common conclusion with us about this feature. Similar to Coroller *et al*.,[20] we found a significant relationship between the variables and purpose. In each of the SPECT-CT and SPECT images, all features selected by the mRMR algorithm had $P < 0.01$. A statistically significant relationship was observed between these features and the target (response to treatment).

Unlike most studies that have used ROC curves and the AUC to evaluate the performance of the classification model, confusion matrixes were employed in the present study. In this study, the target classes are multiclass. In 2020, Sudre *et al*. used radiomics based on dynamic susceptibility contrast (DSC)-MRI to classify gliomas and their mutations and demonstrated the model's performance using a confusion matrix.[34]

Various methods exist for addressing the issue of imbalanced data in the present study. According to Luque's recommendations,[35] we used a decision-tree-based ensemble classifier (RF), DT, and SVM to improve the performance of the model. These classifiers have been considered in many studies to solve the problem of imbalanced data. "KNN" was used in our research due to its simplicity.

As shown in Figure 4, among the predictive models for the features obtained from the SPECT-CT images, RF (ACC = 83%, SN = 77%, and SP = 83%, 94%) performed better than the other classifiers. The next highest rankings were DT (ACC = 79%), KNN (ACC = 74%), and SVM (ACC = 67%). Although the SVM has been proposed to solve the problem of imbalanced data, its accuracy is lower than that of the KNN.

Radiomics analysis of CT images to predict the response to PRRT with ^{177}Lu for comparison with SPECT and CT-SPECT images is done. Three features (dose, LLH-first order uniformity, and LLH-glcm-IMC1) were common to the features of the SPECT-CT dataset. We used the radiomic features of CT images to predict the response to treatment in patients with NETs undergoing PRRT. Modeling of the features obtained from the mRMR pattern showed that the RF and DT algorithms could predict the response to treatment with 74% and 72% accuracy, respectively. The specificity and sensitivity of RF and DT classifiers in the CT images were 91% and 65% and 91% and 64%, respectively.

By examining the performance of the prediction models used for the features extracted from the SPECT images [Figure 5], it was clear that the performances of RF and DT ($ACC_{RF, DT}$ = 64%; $SP_{RF,DT}$ = 88%; SN_{RF} = 59%; SN_{DT} = 58%) were better than that for the other classifiers. SVM and KNN ranked next. The high accuracy of RF compared with the other classifiers is in line with Luque's suggestion for solving the problem of imbalanced data.[35] Outcome prediction in patients with Parkinson's disease using the DaTScan SPECT imaging features was performed by Tang *et al*.[36] In their worrk, 92 imaging and six nonimaging features were extracted from 69 patients, and a leave-one-out strategy combined with artificial neural networks was applied to analyze the data. Combining the top imaging features from the selected regions significantly improves the prediction accuracy to 75%. In 2019, Ahn *et al*. conducted a study that evaluated the prognostic value of ^{18}F-fluorodeoxyglucose in patients with nonsmall-cell lung cancer using the radiomics features of PET images. They utilized different classifiers, such as RF and neural networks, to model the features and evaluated 20 features using the AUC. According to the results, the RF performance had an AUC of 0.956 and an ACC of 0.901, while the neural networks exhibited an AUC of 0.871 and an ACC of 0.780.[37]

A comparison of the performance of the predictive models for CT, SPECT, and SPECT-CT features indicated that the features selected from the SPECT-CT images were more accurate and better described the treatment response. The results [Figures 4 and 5] showed that the RF and DT predictive models performed better than the SVM and KNN models. Regarding the power of predicting the response to treatment, it can be said that SPECT-CT images are better than CT and SPECT images. This difference in accuracy is probably due to the extensive gray levels and high spatial resolution of SPECT-CT images compared with those of SPECT.[38]

In general, by extracting and selecting clinical and imaging features (SPECT-CT images with greater accuracy) through the mRMR pattern and training these features to RF and DT classifiers (owing to better performance), it is possible to determine whether patients with NETs should be treated with ^{177}Lu-DOTATATE. Therefore, one of the most important goals of radiomics, that is, personalization of treatment,[39] can be achieved by facilitating the decision of whether to continue treatment or seek alternative treatments from a specialist. A limitation of the present

study is that the number of studied patients and the number of images taken from them (both SPECT-CT and SPECT) to investigate machine learning were low, owing to the rarity of this type of cancer. In this study CT, images of patients taken from different clinics were used to merge with SPECT images. However, all the images were converted to the same dimensions using the 3D Slicer software before merging. Different imaging protocols and types of scanners can affect the features extracted from the images. It is suggested to use images that are all taken based on the same protocol in future studies. Low accuracy and errors in the fusion of SPECT and CT images can affect the final results. In this study, the modeling of clinical features and quantitative features extracted from images was done simultaneously. In future studies, it is suggested that modeling based on quantitative and qualitative characteristics be done separately to determine which study has better results. Another limitation of the study is the small number of patients due to the rarity of NETs. In future research, with the increase in the number of patients, it is suggested to conduct a more comprehensive study to determine whether the characteristics selected in this study with a small sample size are consistent with the study with a large sample size or not. In future studies, as the number of patients and images increases, deep learning should be used to model the radiomics process because its accuracy is far greater than that of machine learning, and its results are more reliable. Moreover, in the case of an increase in the number of patients with NETs, it is recommended that a distinction be made between them in terms of the type and location of the tumor, and the response to treatment is predicted accordingly. Hence, patients with bone metastases should be separated from those with liver metastases, and the radiomic process should be used for each group to determine which group of patients responds best to the ^{177}Lu-DOTATATE treatment. Finally, it is recommended to employ other medical imaging techniques, such as MRI and whole-body planar imaging, for these patients and to compare the results with those of the present study.

Conclusions

A comparison was made between predicting the response to ^{177}Lu-DOTATATE treatment in patients with NETs based on the radiomics process of SPECT and SPECT-CT images. For both types of images, the mRMR algorithm was used to select the features. Modeling with different machine learning algorithms showed that the RF and DT models could predict treatment responses with optimal accuracy. In terms of image classification, it can be said that using SPECT-CT images can predict the response to treatment, but SPECT images are not suitable for this. Furthermore, the combination of clinical features with quantitative features of SPECT images had no effect on the accuracy and sensitivity of machine learning algorithm models. This combination increased the accuracy and sensitivity of the model in SPECT-CT images. This study showed that radiomics, as a noninvasive and cost-effective method, can be useful for personalized treatment.

Acknowledgment

This study was financially supported by the "Research Department of the School of Medicine, Shahid Beheshti University of Medical Science" (Grant no. 24938).

Financial support and sponsorship

Nil.

Conflicts of interest

There are no conflicts of interest.

References

1. Camus B, Cottereau AS, Palmieri LJ, Dermine S, Tenenbaum F, Brezault C, *et al.* Indications of peptide receptor radionuclide therapy (PRRT) in gastroenteropancreatic and pulmonary neuroendocrine tumors: An updated review. J Clin Med 2021;10:1267.
2. Zhao Z, Bian Y, Jiang H, Fang X, Li J, Cao K, *et al.* CT-radiomic approach to predict G1/2 nonfunctional pancreatic neuroendocrine tumor. Acad Radiol 2020;27:e272-81.
3. Nicolini S, Bodei L, Bongiovanni A, Sansovini M, Grassi I, Ibrahim T, *et al*. Combined use of 177Lu-DOTATATE and metronomic capecitabine (Lu-X) in FDG-positive gastro-entero-pancreatic neuroendocrine tumors. Eur J Nucl Med Mol Imaging 2021;48:3260-7.
4. Feijtel D, Doeswijk GN, Verkaik NS, Haeck JC, Chicco D, Angotti C, *et al.* Inter and intra-tumor somatostatin receptor 2 heterogeneity influences peptide receptor radionuclide therapy response. Theranostics 2021;11:491-505.
5. Dhanani J, Pattison DA, Burge M, Williams J, Riedel B, Hicks RJ, *et al.* Octreotide for resuscitation of cardiac arrest due to carcinoid crisis precipitated by novel peptide receptor radionuclide therapy (PRRT): A case report. J Crit Care 2020;60:319-22.
6. Pavel M, Baudin E, Couvelard A, Krenning E, Öberg K, Steinmüller T, *et al.* ENETS consensus guidelines for the management of patients with liver and other distant metastases from neuroendocrine neoplasms of foregut, midgut, hindgut, and unknown primary. Neuroendocrinology 2012;95:157-76.
7. Kunikowska J, Zemczak A, Kołodziej M, Gut P, Łoń I, Pawlak D, *et al.* Tandem peptide receptor radionuclide therapy using (90)Y/(177)Lu-DOTATATE for neuroendocrine tumors efficacy and side-effects – Polish multicenter experience. Eur J Nucl Med Mol Imaging 2020;47:922-33.
8. Spada F, Campana D, Lamberti G, Laudicella R, Dellamano R, Dellamano L, *et al.* [(177)Lu]Lu-DOTA-TATE versus standard of care in adult patients with gastro-enteropancreatic neuroendocrine tumours (GEP-NETs): A cost-consequence analysis from an Italian hospital perspective. Eur J Nucl Med Mol Imaging 2022;49:2037-48.
9. Bera K, Braman N, Gupta A, Velcheti V, Madabhushi A. Predicting cancer outcomes with radiomics and artificial intelligence in radiology. Nat Rev Clin Oncol 2022;19:132-46.
10. Laudicella R, Comelli A, Liberini V, Vento A, Stefano A, Spataro A, *et al.* [(68)Ga]DOTATOC PET/CT radiomics to

predict the response in GEP-NETs Undergoing [(177)Lu] DOTATOC PRRT: The "theragnomics" concept. Cancers (Basel) 2022;14:984.
11. Horvat N, Bates DD, Petkovska I. Novel imaging techniques of rectal cancer: What do radiomics and radiogenomics have to offer? A literature review. Abdom Radiol (NY) 2019;44:3764-74.
12. Avanzo M, Stancanello J, El Naqa I. Beyond imaging: The promise of radiomics. Phys Med 2017;38:122-39.
13. Xu J, Yang J, Feng Y, Zhang J, Zhang Y, Chang S, *et al.* MRI feature-based nomogram model for discrimination between non-hypervascular pancreatic neuroendocrine tumors and pancreatic ductal adenocarcinomas. Front Oncol 2022;12:856306.
14. Zhang T, Xiang Y, Wang H, Yun H, Liu Y, Wang X, *et al.* Radiomics combined with multiple machine learning algorithms in differentiating pancreatic ductal adenocarcinoma from pancreatic neuroendocrine tumor: More hands produce a stronger flame. J Clin Med 2022;11:6789.
15. Ma J, Wang X, Tang M, Zhang C. Preoperative prediction of pancreatic neuroendocrine tumor grade based on (68) Ga-DOTATATE PET/CT. Endocrine 2024;83:502-10.
16. Alibabaei S, Rahmani M, Tahmasbi M, Tahmasebi Birgani MJ, Razmjoo S. Evaluating the gray level co-occurrence matrix-based texture features of magnetic resonance images for glioblastoma multiform patients' treatment response assessment. J Med Signals Sens 2023;13:261-71.
17. Dehghani F, Karimian A, Arabi H. Joint brain tumor segmentation from multi magnetic resonance sequences through a deep convolutional neural network. J Med Signals Sens 2024:14:9.
18. Behmanesh B, Abdi-Saray A, Deevband MR, Amoui M, Haghighatkhah HR. Radiomics analysis for clinical decision support in 177lu-dotatate therapy of metastatic neuroendocrine tumors using CT images. Biomed Phys Eng 2022. Available from: https://www.jbpe.sums.ac.ir/article_48455.html. [Last accessed on 2022 Jun 15]. doi: 10.31661/jbpe.v0i0.2112-1444.
19. Biomarkers Definitions Working Group. Biomarkers and surrogate endpoints: Preferred definitions and conceptual framework. Clin Pharmacol Ther 2001;69:89-95.
20. Coroller TP, Grossmann P, Hou Y, Rios Velazquez E, Leijenaar RT, Hermann G, *et al.* CT-based radiomic signature predicts distant metastasis in lung adenocarcinoma. Radiother Oncol 2015;114:345-50.
21. Kolossváry M, Kellermayer M, Merkely B, Maurovich-Horvat P. Cardiac computed tomography radiomics: A comprehensive review on radiomic techniques. J Thorac Imaging 2018;33:26-34.
22. Ding C, Han H, Li Q, Yang X, Liu T. iT3SE PX: Identification of bacterial type III secreted effectors using PSSM profiles and XGBoost feature selection. Comput Math Methods Med 2021:6690299.
23. Peng H, Long F, Ding C. Feature selection based on mutual information: Criteria of max-dependency, max-relevance, and min-redundancy. IEEE Trans Pattern Anal Mach Intell 2005;27:1226-38.
24. Cai Y, Huang T, Hu L, Shi X, Xie L, Li Y. Prediction of lysine ubiquitination with mRMR feature selection and analysis. Amino Acids 2012;42:1387-95.
25. Igual L, Seguí S, editors. Supervised learning BT – Introduction to data science. In: A Python Approach to Concepts, Techniques and Applications. Cham: Springer International Publishing; 2024. p. 67-97.
26. Dese K, Raj H, Ayana G, Yemane T, Adissu W, Krishnamoorthy J, *et al.* Accurate machine-learning-based classification of leukemia from blood smear images. Clin Lymphoma Myeloma Leuk 2021;21:e903-14.
27. Chern CC, Lei WU, Huang KL, Chen SY. A decision tree classifier for credit assessment problems in big data environments. Inf Syst E-bus Manag 2021;19:363-86.
28. Prabha A, Yadav J, Rani A, Singh V. Design of intelligent diabetes mellitus detection system using hybrid feature selection based XGBoost classifier. Comput Biol Med 2021;136:104664.
29. Heydarian M, Doyle TE, Samavi R. MLCM: Multi-label confusion matrix. IEEE Access 2022;10:19083-95.
30. Liu C, Bian Y, Meng Y, Liu F, Cao K, Zhang H, *et al.* Preoperative prediction of G1 and G2/3 grades in patients with nonfunctional pancreatic neuroendocrine tumors using multimodality imaging. Acad Radiol 2022;29:e49-60.
31. Song T, Zhang QW, Duan SF, Bian Y, Hao Q, Xing PY, *et al*. MRI-based radiomics approach for differentiation of hypovascular non-functional pancreatic neuroendocrine tumors and solid pseudopapillary neoplasms of the pancreas. BMC Med Imaging 2021;21:36.
32. Huynh E, Coroller TP, Narayan V, Agrawal V, Hou Y, Romano J, *et al.* CT-based radiomic analysis of stereotactic body radiation therapy patients with lung cancer. Radiother Oncol 2016;120:258-66.
33. Liberini V, Rampado O, Gallio E, De Santi B, Ceci F, Dionisi B, *et al.* (68)Ga-DOTATOC PET/CT-based radiomic analysis and PRRT outcome: A preliminary evaluation based on an exploratory radiomic analysis on two patients. Front Med (Lausanne) 2020;7:601853.
34. Sudre CH, Panovska-Griffiths J, Sanverdi E, Brandner S, Katsaros VK, Stranjalis G, *et al*. Machine learning assisted DSC-MRI radiomics as a tool for glioma classification by grade and mutation status. BMC Med Inform Decis Mak 2020;20:149.
35. Carrasco A, Martín A, de las Heras A. The impact of class imbalance in classification performance metrics based on the binary confusion matrix, Pattern Recognition 2019;91:216-31.
36. Tang J, Yang B, Adams MP, Shenkov NN, Klyuzhin IS, Fotouhi S, *et al.* Artificial neural network-based prediction of outcome in parkinson's disease patients using DaTscan SPECT imaging features. Mol Imaging Biol 2019;21:1165-73.
37. Ahn HK, Lee H, Kim SG, Hyun SH. Pre-treatment (18)F-FDG PET-based radiomics predict survival in resected non-small cell lung cancer. Clin Radiol 2019;74:467-73.
38. Ritt P. Recent developments in SPECT/CT. Semin Nucl Med 2022;52:276-85.
39. Sala E, Mema E, Himoto Y, Veeraraghavan H, Brenton JD, Snyder A, *et al.* Unravelling tumour heterogeneity using next-generation imaging: Radiomics, radiogenomics, and habitat imaging. Clin Radiol 2017;72:3-10.